Internal variability of the climate system mirrored in decadal-scale trends of surface solar radiation

Boriana Chtirkova[1], Doris Folini[1], Lucas Ferreira Correa[1], and Martin Wild[1]

[1]ETH Zürich

April 27, 2023

Posted on 9 Feb 2023 — The copyright holder is the author/funder. All rights reserved. No reuse without permission. — https://doi.org/10.22541/essoar.167591116.63130694/v1 — This a preprint and has not been peer reviewed. Data may be preliminary.

Internal variability of the climate system mirrored in decadal-scale trends of surface solar radiation

Boriana Chtirkova[1], Doris Folini[1], Lucas Ferreira Correa[1], Martin Wild[1]

[1]Institute for Atmospheric and Climate Sciences, ETH Zürich, Zürich, Switzerland

Key Points:

- Long term trends in annual mean all-sky and clear-sky surface solar radiation entail strong changes in major climate indices.
- Annual mean surface solar radiation variability is 25% to 30% more for variable in time than for climatological sea surface temperatures.
- Constantly higher aerosol loads result in increased variability for clear-sky conditions, but not for all-sky conditions.

Corresponding author: Boriana Chtirkova, `boriana.chtirkova@env.ethz.ch`

Abstract

Decadal-scale unforced climate variability associated with low-frequency ocean (or coupled) modes can be identified within the time-evolving sea surface temperature (SST) pattern. We seek to find a relationship between 12 well-known climate modes of variability (ENSO, PDO, AMO, etc.), which are reflected in the SST pattern, and decadal trends in downwelling shortwave radiation at Earth's surface (surface solar radiation, SSR). The analysis is performed using the pre-industrial control runs (piControl) of 57 models from the Coupled Model Intercomparison Project – Phase 6. We find that regional SSR trends occur during periods when a climate mode is transitioning and show a mirroring pattern (opposite sign SSR trends) when the mode transitions in the opposite direction. Unforced trends in clear-sky SSR are mostly driven by SST-induced water vapour changes, while all-sky SSR trends show a complex spatial structure with trends of different signs in different regions. Unforced SSR trends are generally weaker in simulations with climatological SSTs. The role of natural aerosols as another potentially relevant factor for SSR variability is briefly addressed and we find that constantly higher aerosol loads result in increased variability for clear-sky conditions, but not for all-sky conditions. The results from this study suggest that all-sky dimming and brightening in different parts of the world was enhanced rather than suppressed by internal variability related to the SST-pattern with the exception of India and China, where both effects are present. A practical application can be the planning of photovoltaic energy facilities given areas where internal variability is generally smaller or affects SSR in opposite directions.

Plain Language Summary

The Earth system (atmosphere, ocean, land, cryoshpere and biosphere) changes not only as a result of anthropogenic or volcanic activities but also as a result of internal processes, also known as background noise. Climate science offers a simplified description of this "noise" by assigning climate indices, which help to describe the larger system with a single time series. More generally, the climate indices are an attempt to describe the temporal evolution of complex modes of variability such as El Niño–Southern Oscillation (ENSO), Pacific Decadal Oscillation (PDO), Atlantic Multidecadal Oscillation (AMO). With the use of climate models, we check how these indices are reflected in the decadal changes of solar radiation reaching Earth's surface, a flux which is mainly affected by clouds, water vapour, and natural and anthropogenic aerosols suspended in the atmosphere. Our results suggest that ocean surface temperature changes, which evolve over a few decades, control cloudiness and water vapour amounts above many land regions. This ocean temperature evolution may result in a naturally-induced dimming and brightening of solar radiation over continents. Our findings are relevant for questions involving long-term changes of the solar radiation reaching the Earth's surface, ranging from physical causes of observed changes to long term planning of photovoltaic energy production.

1 Introduction

Decadal-scale unforced variability of the climate system is mostly associated with patterns in sea surface temperature (SST) changes (Deser, Alexander, et al., 2010) as the ocean, being a slower component of the climate system, is able to exhibit modes of variability on such temporal scales. This climate system variability is reflected in variations in the different energy budget components such as the shortwave and longwave radiative fluxes at the surface and the top of the atmosphere (TOA). Many aspects of climate variability, i.e. the SST pattern, can be traced back to different modes of variabiltiy such as El Niño–Southern Oscillation (ENSO), Pacific Decadal Oscillation (PDO), Atlantic Multidecadal Oscillation (AMO), etc. A convenient way to describe the temporal evolution of these modes of climate variability in time are their corresponding climate indices (Nino3.4 index, PDO index, AMO index), which are usually computed upon the SST anomaly. The effects of ENSO and PDO on the Earth's radiative budget have been investigated in Loeb et al. (2012, 2018), where the regional distribution of the TOA shortwave flux is shown to match an SST pattern representative for PDO and tropical variations in outgoing longwave radiation are found to closely track changes in ENSO. Through radiation feedbacks and large-scale dynamics, ENSO is also shown to affect the hydrological cycle (Stephens et al., 2018). Pinker et al. (2017) estimate that the anomalous downwelling surface shortwave radiation (SSR) associated with an ENSO event can reach up to 60 Wm^{-2} (monthly anomaly for January 1987 in the Western Pacific warm pool region) and that the location of the largest SSR anomaly coincides with the area of largest anomalous SST gradient as also described in Lindzen and Nigam (1987). Despite its primarily 3-7 year time scale, ENSO is found to be the mode of variability with the largest impact on TOA energy balance and global radiative feedback even on decadal time scales (Wills et al., 2021).

From a surface perspective, long term observations indicate decadal scale trends in SSR in many locations; these changes of the downwelling shortwave flux at Earth's surface are termed dimming and brightening (Wild et al., 2005). The similarity between the temporal scales of dimming/brightening and PDO and AMO cycles has been noted in Wild (2012). These changes in SSR have been observed in both all-sky and clear-sky conditions: within the United States, Augustine and Hodges (2021) suggest that cloud cover was the primary cause for brightening ($+7.36\ \mathrm{Wm}^{-2}\mathrm{decade}^{-1}$ during 1996-2012) and dimming ($-3.90\ \mathrm{Wm}^{-2}\mathrm{decade}^{-1}$ during 2012-2019); for Europe, Wild et al. (2021) provide evidence for all-sky and clear-sky dimming and brightening of similar magnitudes (order of 10 Wm-2decade^{-1}). Different underlying causes are discussed in the literature. One widely accepted cause is changing anthropogenic aerosol emission, acting either directly on SSR or via cloud-aerosol effects (e.g. Streets et al. (2006); Wild (2009)). Another suggested relevant factor is internal variability of the climate system, acting on SSR notably but not exclusively via clouds. Within observations, Augustine and Capotondi (2022) suggest leading ocean modes in the Pacific (PDO) and Atlantic (AMO) oceans as the prime driver for dimming and brightening over the Northern Hemispheric continents through influencing upper level pressure fields and thus cloud formation.

Modelling studies help us gain an understanding of the relevance of SSTs for simulating changes in the radiative fluxes. To see how temporally varying SSTs affect the climate, modelling studies often compare simulations where SSTs vary both seasonally and year-to-year with simulations where SSTs are kept constant year-to-year but still exhibit the seasonal cycle, i.e. climatological SSTs. For example, Folini and Wild (2015) find that the ceasing of SSR dimming over China around the year 2000 cannot be simulated with climatological SSTs but cloud-cover changes induced by time-varying SSTs are key for the SSR recovery. With a TOA perspective, Loeb et al. (2020) show that observed TOA fluxes can be represented in atmosphere-only simulations with prescribed observational SSTs as compared to fully-coupled climate simulations with freely evolving SSTs, suggesting that the effect of SSTs on radiative fluxes in the observational period has been crucial.

This study seeks to further explore the connection between SST and SSR both above land and oceans within a climate without external forcings – neither anthropogenic, nor natural (e.g. volcanic). We focus on internal variability of SSR, specifically asking about the role of unforced SST variability for SSR variability from global to regional scale. We address the following questions: How strongly is SSR variability reduced if SSTs are climatological instead of time-evolving (Section 3.1)? How does the effect from unforced SSTs compare with that from natural aerosols, notably dimethyl sulfate (DMS), dust, and sea salt (Section 3.2)? Assuming that long-term and global-scale natural climate variability can be well described by the known modes of variability, we check whether well-known modes which reflect SST variability leave an imprint on SSR (Section 3.3). The focus is on the following climate modes: El Niño–Southern Oscillation (ENSO), Interdecadal Pacific Oscillation (IPO), Pacific Decadal Oscillation (PDO), Atlantic Multidecadal Oscillation (AMO), Atlantic Meridional Mode (AMM), Atlantic Niño (ATL3), North Tropical Atlantic (NTA), South Tropical Atlantic (STA), Indian Ocean Dipole (IOD), Tropical Indian Ocean (TIO), Southern Ocean mode (SO). These modes should generally be representative of long-term variations in the SST field and are quantified by their corresponding climate index.

The range of possible SSR trends (positive and negative) solely caused by internal variability has been quantified in Folini et al. (2017) and Chtirkova et al. (2022) based on unforced long-term climate simulations. The present paper aims at further constraining how internal variability affects SSR trends at different locations through the SST pattern or through aerosols. The structure is as follows: in section 2, we describe the data (section 2.1), the methods used to quantify the role of SSTs (section 2.2) and methods used to quantify the role of aerosols (section 2.3) for SSR internal variability; results regarding the general role of SSTs are given in section 3.1, results related to aerosols - in section 3.2 and the specific effect of different modes of variability (AMO, PDO, etc.) on SSR trends - in section 3.3; we discuss the representation of decadal variability in climate models (section 4.1), the applicability of the results based on pre-industrial climate to present-day (section 4.2) and the relationship to dimming and brightening (section 4.3).

2 Data and Methods

We make ample use of Coupled model intercomparison project – CMIP6 data (Eyring et al., 2016) to look at unforced SSR variability and relate it to well-known modes of SST variability. In doing so, we rely on findings by Fasullo et al. (2020) and Coburn and Pryor (2021), who examined the ability of CMIP6 models to represent specific modes of climate variability and found an overall improvement of associated model performance with each CMIP generation. We discuss our results in view of their findings in Section 4. Parts of this study further rely on findings by Folini et al. (2017) and Chtirkova et al. (2022), who demonstrated that quantitative estimates of unforced SSR trends of arbitrary (decadal-scale) length and statistical significance can be obtained from the standard deviation σ_{SSR} of the underlying (unforced) annual mean SSR time series. In addition, we check whether σ_{SSR} would be different if the mean SSR is artificially reduced by increasing the amount of forcing constituents in the atmosphere, namely natural and anthropogenic aerosols.

2.1 CMIP6 data

The backbone of this study is formed by the fully coupled pre-industrial control simulations (piControl, 57 models) and their atmosphere-only counterparts (piClim-control, 21 models), which we use to quantify the effect of time varying SSTs on SSR. In addition, to examine the role of different aerosol constituents for SSR variability, we use of AerChemMIP and RFMIP endorsed experiments. These are atmosphere (and land)-only runs with climatological SSTs, which simulate a pre-industrial climate with a change in a single atmospheric forcing constituent (for example doubling the amount of sea salt). The CMIP6-endorsed experiments relevant for our study are summarized in Table 1. The models with simulations available for the different experiments are listed in Table 2. Our analysis uses annual mean data and is performed on a per grid box level on the native grid of each model. Multi-model median maps are computed via interpolation from each model's native grid to a 1°grid and associated quantities are denoted by an over-bar.

The comprehensive set of CMIP6 models we use may raise concerns that in this way models with improper representation of variability are included as well, which potentially contaminate results. To address this concern, we repeated part of the analysis with a subset of 14 models that perform well in simulating these aspects of variability according to Fasullo et al. (2020). As this performance analysis does not specifically evaluate decadal scale SSR trends, as are of interest here, we repeated part of the analysis also with 6 random draws of 14 simulations each out of the 69 piControl simulations available. These additional analysis, detailed in Supplementary Information (Part 1), all demonstrate that the presented results based on all available CMIP6 data are robust.

Table 1. CMIP6 endorsed experiments used in the study. All experiments represent a pre-industrial climate. Fourth column indicates whether the experiment involves an ESM with time evolving (coupled) or prescribed climatological sea surface temperatures (SST) and sea ice concentrations (SIC).

Experiment	# of models	# of models and ensembles	SST and SIC	Endorsed by	Length [years]	Description
piControl	57	69	coupled	DECK	>500	Control, fully-coupled (FC)
piClim-control	21	24	pres. clim.	AerChemMIP, RFMIP	30	Control, atmosphere-only (AO)
piClim-2xDMS	6	7	pres. clim.	AerChemMIP	30	AO with doubled emissions of DMS
piClim-2xdust	9	10	pres. clim.	AerChemMIP	30	AO with doubled emissions of dust
piClim-2xfire	5	5	pres. clim.	AerChemMIP	30	AO with doubled emissions from fires
piClim-2xss	8	9	pres. clim.	AerChemMIP	30	AO with doubled emissions of sea salt
piClim-4xCO2	18	25	pres. clim.	RFMIP	30	AO, effective radiative forcing by 4xCO2
piClim-BC	10	11	pres. clim.	AerChemMIP	30	AO with 2014 black carbon emissions
piclim-OC	9	11	pres. clim.	AerChemMIP	30	AO with 2014 organic carbon emissions
piClim-SO2	10	12	pres. clim.	AerChemMIP	30	AO with 2014 SO2 emissions
piClim-aer	21	30	pres. clim.	AerChemMIP, RFMIP	30	AO with 2014 aerosol emissions

Table 2. Models included in each CMIP6 endorsed experiment.

	piControl	piClim-control	piClim-2xDMS	piClim-2xdust	piClim-2xfire	piClim-2xss	piClim-4xCO2	piClim-BC	piClim-OC	piClim-SO2	piClim-aer
ACCESS-CM2	yes	yes	-	-	-	-	yes	-	-	-	yes
ACCESS-ESM1-5	yes	yes	-	-	-	-	yes	-	-	-	yes
AWI-CM-1-1-MR	yes	-	-	-	-	-	-	-	-	-	-
AWI-ESM-1-1-LR	yes	-	-	-	-	-	-	-	-	-	-
BCC-CSM2-MR	yes	-	-	-	-	-	-	-	-	-	-
BCC-ESM1	yes	yes	-	-	-	-	-	yes	-	yes	yes
CAS-ESM2-0	yes	-	-	-	-	-	-	-	-	-	-
CESM2	yes	yes	-	-	-	-	yes	-	-	-	yes
CESM2-FV2	yes	-	-	-	-	-	-	-	-	-	-
CESM2-WACCM	yes	yes	-	-	-	-	-	-	-	-	-
CESM2-WACCM-FV2	yes	-	-	-	-	-	-	-	-	-	-
CIESM	yes	-	-	-	-	-	-	-	-	-	-
CMCC-CM2-SR5	yes	-	-	-	-	-	-	-	-	-	-
CMCC-ESM2	yes	-	-	-	-	-	-	-	-	-	-
CNRM-CM6-1	yes	yes	-	-	-	-	yes	-	-	-	yes
CNRM-CM6-1-HR	yes	-	-	-	-	-	-	-	-	-	-
CNRM-ESM2-1	yes	yes	yes	yes	yes	yes	yes	yes	yes	yes	yes
CanESM5	yes	yes	-	-	-	-	yes	-	-	-	yes
CanESM5-CanOE	yes	-	-	-	-	-	-	-	-	-	-
E3SM-1-0	yes	-	-	-	-	-	-	-	-	-	-
E3SM-1-1	yes	-	-	-	-	-	-	-	-	-	-
E3SM-1-1-ECA	yes	-	-	-	-	-	-	-	-	-	-
EC-Earth3	yes	yes	yes	yes	-	-	yes	-	-	-	yes
EC-Earth3-AerChem	yes	yes	yes	yes	-	-	-	-	-	-	yes
EC-Earth3-CC	yes	-	-	-	-	-	-	-	-	-	-
EC-Earth3-LR	yes	-	-	-	-	-	-	-	-	-	-
FGOALS-f3-L	yes	-	-	-	-	-	-	-	-	-	-
FGOALS-g3	yes	-	-	-	-	-	-	-	-	-	-
GFDL-CM4	yes	yes	-	-	-	-	yes	-	-	-	yes
GFDL-ESM4	yes	yes	-	yes	-	yes	yes	yes	yes	yes	yes
GISS-E2-1-G	yes	yes	yes	yes	yes	yes	yes	yes	yes	yes	yes
GISS-E2-1-H	yes	-	-	-	-	-	-	-	-	-	-
GISS-E2-2-G	yes	-	-	-	-	-	-	-	-	-	-
HadGEM3-GC31-LL	yes	yes	-	-	-	-	yes	-	-	-	yes
HadGEM3-GC31-MM	yes	-	-	-	-	-	-	-	-	-	-
IITM-ESM	yes	-	-	-	-	-	-	-	-	-	-
INM-CM4-8	yes	-	-	-	-	-	-	-	-	-	-
INM-CM5-0	yes	-	-	-	-	-	-	-	-	-	-
IPSL-CM5A2-INCA	yes	-	-	-	-	-	-	-	-	-	-
IPSL-CM6A-LR	yes	yes	-	yes	-	yes	yes	yes	yes	yes	yes
KACE-1-0-G	yes	-	-	-	-	-	-	-	-	-	-
MIROC-ES2H	yes	yes	-	-	-	-	-	-	-	-	-
MIROC-ES2L	yes	-	-	-	-	-	-	-	-	-	-
MIROC6	yes	yes	-	yes	yes	yes	yes	yes	yes	yes	yes
MPI-ESM-1-2-HAM	yes	yes	yes	yes	yes	yes	-	yes	yes	yes	yes
MPI-ESM1-2-HR	yes	yes	-	-	-	-	-	-	-	-	-
MPI-ESM1-2-LR	yes	yes	-	-	-	-	yes	-	-	-	-
MRI-ESM2-0	yes	yes	-	-	-	-	yes	yes	yes	yes	yes
NESM3	yes	-	-	-	-	-	-	-	-	-	-
NorCPM1	yes	-	-	-	-	-	-	-	-	-	-
NorESM1-F	yes	-	-	-	-	-	-	-	-	-	-
NorESM2-LM	yes	yes	yes	yes	-	yes	yes	yes	yes	yes	yes
NorESM2-MM	yes	yes	-	-	-	-	yes	-	-	-	yes
SAM0-UNICON	yes	-	-	-	-	-	-	-	-	-	-
TaiESM1	yes	yes	-	-	-	-	-	-	-	-	-
UKESM1-0-LL	yes	yes	yes	yes	yes	yes	yes	yes	yes	yes	yes

2.2 Quantifying the role of SSTs for SSR variability

We examine the potential imprint of unforced SST variability on SSR variability and associated unforced trends from two perspectives. Step one is to ask whether and where on the globe the magnitude of σ_{SSR} is different, depending on whether SSTs are time variable (piControl) or climatological (piClim-Control). Step two is to examine whether decadal scale SSR trends mirror the temporal changes of selected SST patterns, such as the Pacific Decadal Oscillation (PDO).

To quantify the overall role of time variable SSTs in SSR variability (first step above), we consider those 21 models that have data for both, the piControl and piClim-control experiment. For each model, we compute at the grid box level the SSR variability of either experiment, σ_{SSR}(piControl) and σ_{SSR}(piClim-control). We next take the multi-model median for each experiment separately, $\bar{\sigma}_{SSR}$(piControl) and $\bar{\sigma}_{SSR}$(piClim-control), after remapping all models on a common 1°grid. Finally, we combine the two multi-model median maps into a map of relative change in SSR variability $\bar{\sigma}_{SSR,rel} = (\bar{\sigma}_{SSR}(\text{piControl}) - \bar{\sigma}_{SSR}(\text{piClim-control}))/\bar{\sigma}_{SSR}(\text{piClim-control})$.

Regarding the potential imprint of changing SST patterns on unforced SSR trends (second step above), we examine a selection of well established SST patterns:

- Atlantic Multidecadal Oscillation (AMO)
- Atlantic Meridional Mode (AMM)
- Atlantic Niño (ATL3), also known as Atlantic Zonal Mode (AZM)
- North Tropical Atlantic (NTA)
- South Tropical Atlantic (STA)
- Indian Ocean Dipole (IOD)
- Tropical Indian Ocean (TIO), also known as Indian Ocean Basin (IOB)
- El Niño and Southern Oscillation (ENSO), described by Nino3.4 index
- Pacific Decadal Oscillation (PDO)
- Interdecadal Pacific Oscillation (IPO)
- Southern Ocean (SO)
- Global SST (global SST)

Taken together these modes cover all major ocean basins. Moreover, they cover both meridional and zonal modes, with an associated tendency to couple to the Hadley and Walker circulation, respectively. Based on this coupling of SST patterns and atmospheric circulation, we hypothesize that a strong change over a time window of N years in any of these SST patterns may result in an associated, strong change in SSR in at least some regions. We test our hypothesis on data from 69 CMIP6 simulations (from 57 models) that provide fully coupled pre-industrial (piControl) simulations; the analysis is conducted separately for time windows of $N = 10$, 20, and 30 years.

We compute from monthly mean data for each of the 69 piControl simulations the climate indices associated with the above listed SST patterns, using The Climate Variability Diagnostics Package – CVDP, version 5.1.1 (Phillips et al., 2014), developed by NCAR's Climate Analysis Section. By construction, a strong change in a pattern specific index is indicative of a strong change in the SST pattern itself, typically from 'positive' to 'negative' phase or vice versa. A brief illustration of the method is given in Figure 1. To identify in the annual mean index time series those N-year periods with the strongest index change (increase or decrease), we compute all possible (overlapping) N year trends (linear regressions) in the index time series (Figure 1 a), assemble them in a histogram (Figure 1 b), and identify the N-year periods of the trends in the upper- and lower-most 10% of the distribution. For the example case illustrated on Figure 1 with 500 years of data, this corresponds to 50 30-year periods with a negative trend and 50 30-year periods with a positive trend. For these periods (indicated as red lines on Fig-

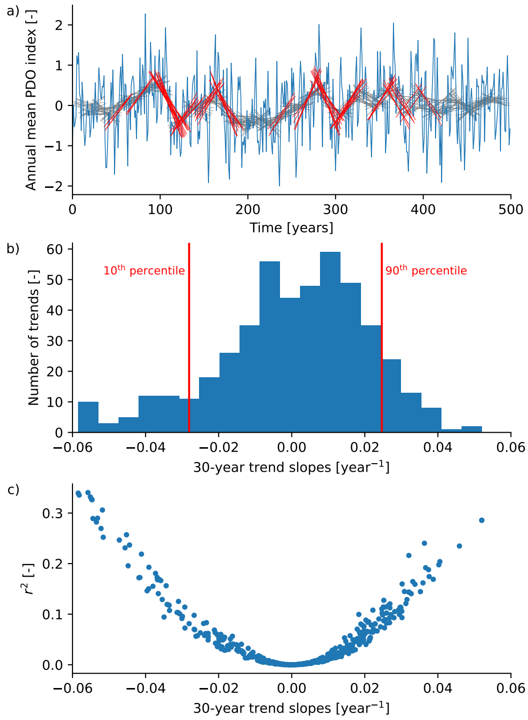

Figure 1. An illustration of the method which consists of taking the time series of a climate index (a), calculating all possible N-year trends as linear regressions (thin gray lines) and taking the trends larger than the 90th percentile and smaller than the 10th percentile of the distribution (thick red lines); a histogram of the distribution of N-year trends is shown on (b) with vertical red lines marking the 10th and 90th percentiles. Bottom-most plot (c) shows the coefficient of determination (r^2) from the linear fit for each trend value (same x-axis in (b) and (c)). The model used for the illustration is GFDL-ESM4, the climate index is PDO and the trend length is 30 years.

ure 1, either with a positive or a negative slope), we extract grid box specific SSR trends for each of these periods and combine them into a composite (mean) trend - one for the increasing and one for the decreasing phases of the SST index, respectively. This is done individually for each of the 69 piControl simulations, yielding two SSR trend maps (for positive and negative trends) per index for each model (the trend maps for individual models are included in Supplementary Information – Part 2). In order to obtain multi-model maps, we further normalize these maps of the individual models by mapping the range from minimum to maximum SSR trend (among all possible SSR trends for the specific grid box) to [-1, 1]. This normalization is done because our method of selecting percentiles from the index distribution does not account for different amplitudes of variability of the climate modes and thus we cannot expect they yield similar magnitudes for SSR trends; further, many climate indices are normalized by their variance by definition and thus similar climate index values may correspond to different underlying SST anomalies (within the different models); these two reasons lead to a large inter-model difference with respect to the obtained SSR trends, which is to be overcome by normalization. Finally, we take the multi-model mean of the normalized SSR trends (after re-mapping to our common 1°grid). Thereby we obtain for each SST mode two composite maps (per N-year trends analysis) that show the normalized SSR trend pattern for phases of strongest

SST index increase and decrease, respectively. The resulting maps show the SSR trends based on periods with strong unforced SST trends.

A region specific discussion of the connection, if any, between strong changes in an SST index and SSR trends is desirable. The regions (land only) we select by visual inspection of SSR trend maps (that are derived from SST index trends), focusing on regions that do show SSR trends upon strong changes of at least some SST indices. For each region, we follow our data analysis procedure to the point when we have non-normalized per grid box per model composite trends (computed from the aggregated time series) for phases of strongest SST index increase and decrease, respectively. Then we take the regional mean of the trends for each model and count the number of models whose trend magnitude t falls within a prescribed range. For $N = 20$ year all-sky and clear-sky trends, we choose these ranges as $t > 1$, $t > 0.5$, $t > 0$ Wm^{-2}decade^{-1} (negative for decreasing trends).

2.3 Quantifying the role of aerosols for SSR variability

Aerosols are another potential factor affecting SSR variability and CMIP6 offers experiments dedicated to the role of aerosols in selected aspects of the climate system. The available database does, however, not allow for an identical analysis and hypothesis testing as in the case of SSTs. Experiments where the same model is run with fixed (climatological) as well as with time varying (due to internal variability) AOD are missing. What can be done with the available data is to distinguish between regions that are more or less prone to natural aerosols affecting the internal variability of SSR.

We basically compare each of the different piClim experiments listed in Table 1 with piClim-Control. If in such a comparison only a subset of models is available for the piClim experiment, the same subset is used for the piClim-Control data. For each piClim experiment and its piClim-control counter part, we compute multi-model median maps of the SSR long-term (30 years) mean and standard deviation. The former (long-term mean SSR) we use to identify regions where natural aerosol emissions potentially affect SSR variability. The latter (SSR variability) we use to examine whether the magnitude of SSR variability is sensitive to absolute amounts of aerosol (relative change in variability, $\bar{\sigma}_{SSR,rel} = (\bar{\sigma}_{SSR}(\text{piClim}) - \bar{\sigma}_{SSR}(\text{piClim-control}))/\bar{\sigma}_{SSR}(\text{piClim-control}))$. We also apply the same analysis to CMIP6 piClim experiments dedicated to anthropogenic aerosols as well as quadroupling of CO_2.

3 Results

The results are organised as follows: first we check whether and where inter-annual SST variability is of relevance for SSR variability, thus also unforced SSR trends; second, we check where on the globe SSR variability may be affected by individual aerosol species; lastly, we again turn to SST variability, now linking known SST-related climate modes of variability with SSR trends.

3.1 The role of time-evolving SSTs for SSR variability

To investigate whether and where any pattern of time-evolving SSTs are relevant for inter-annual SSR variability, we compare SSR variability from a fully-coupled CMIP6 experiment with time-evolving SSTs (piControl) and an atmosphere-only experiment with pre-industrial climatological SSTs (piClim-Control). The latter experiment has a multi-model global mean SSR variability of 3.93 ± 1.04 Wm^{-2} and 0.56 ± 0.28 Wm^{-2} in all sky and clear sky, respectively, which must be due to causes other than time varying SSTs (uncertainty estimate is based on the CMIP6 multi-model spread; spread is defined as the difference between the 90$^{\text{th}}$ and 10$^{\text{th}}$ percentiles of all models). The global average change between piControl and piClim-Control in σ_{SSR} over all models is 1 Wm^{-2} for

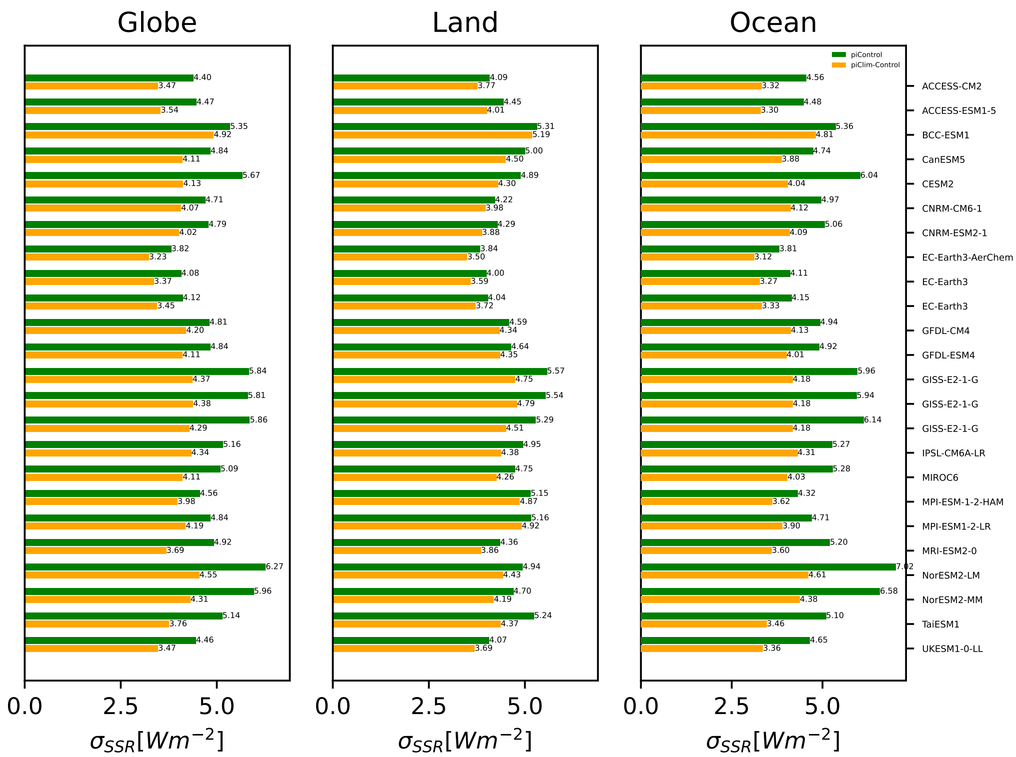

Figure 2. Variability of annual mean all-sky SSR in a coupled atmosphere-ocean system (data from piControl) and a system with climatological SSTs (data from piClim-control) per model. σ_{SSR} averaged over the globe (left), averaged over land ares only (middle), and averaged over oceans (right). Data is area-weighted on the native model grids.

all-sky and 0.2 Wm^{-2} for clear sky SSR. To assess where on the globe this difference is statistically significant, we proceed as follows: for each grid box, we assemble the data of the 24 CMIP6 models into two distribution functions of σ_{SSR}, one for piControl, the other for piClim-Control. To test our null hypothesis – that piControl and piClim-Control are the same in a specific grid box – we use the Mann-Whitney U test (Mann & Whitney, 1947). We find that the null hypothesis is rejected at the 5% confidence level for 56% for all-sky, 57% for clear-sky SSR, of grid boxes; areas where the test is rejected are left unhatched on Figure 3. In units relative to the global mean $\bar{\sigma}_{SSR}$, these correspond to a 25% increase in all-sky SSR variability and a 30% increase in clear-sky SSR variability when including time-evolving SSTs into the system. Figure 2 shows per model box plots for all-sky σ_{SSR} averaged over the globe, land-areas only and only above oceans – the global increase in variability in the coupled atmosphere-ocean system is mostly but not only due to increased variability above oceans.

To further investigate where on the globe SST variability and inter-annual SSR variability are connected, we show in Figure 3 maps of the magnitude of $\bar{\sigma}_{SSR}$ for piClim-control as well as maps of the relative change of $\bar{\sigma}_{SSR}$: $\bar{\sigma}_{SSR,rel}$. The values are based on the multi-model median of models participating in the piClim-control experiment (see Table 2). Maps of $\bar{\sigma}_{SSR}$(piClim-control) (Figure 3 a, c) show substantial, spatially inhomogenous SSR variability already for pre-industrial conditions with prescribed climatological SSTs. Clear-sky variability suggests an imprint from land masses, especially desert regions. All-sky variability suggests an imprint of monsoon systems (see e.g. Yim

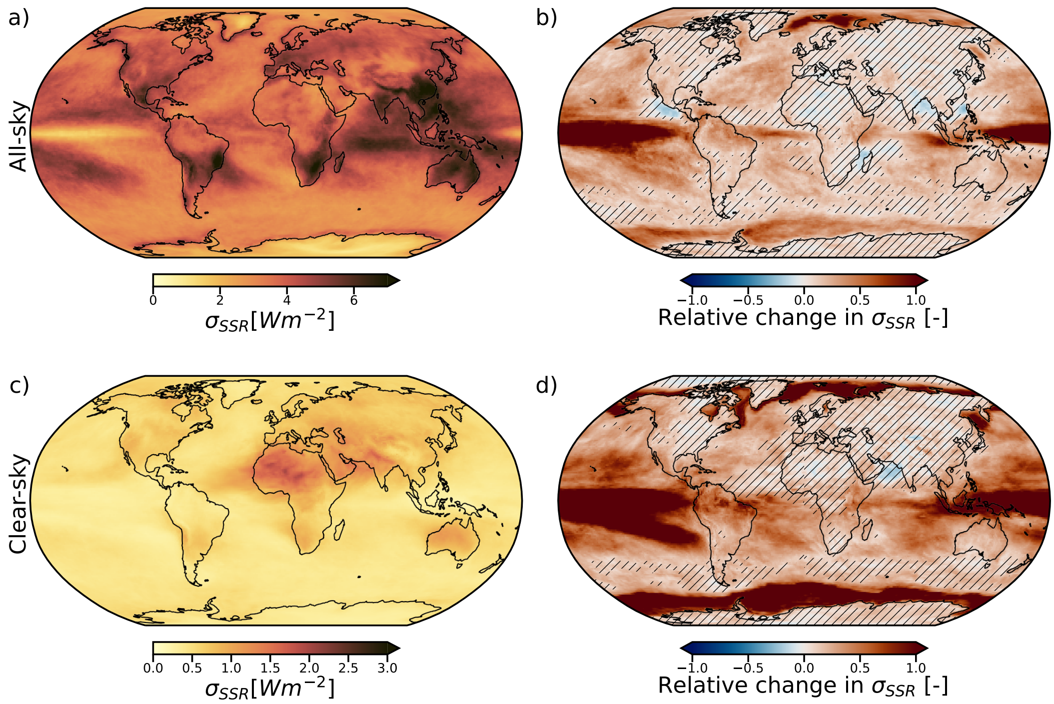

Figure 3. Variability of SSR in a system with prescribed climatological SSTs (piClim-control) for all-sky (a) and clear-sky SSR (c). Right panels (b and d) show the relative change in $\bar{\sigma}_{SSR}$ when time-evolving SSTs apply instead (the absolute difference, divided by $\bar{\sigma}_{SSR}$(piClim-control) per grid box) – red areas indicate time-evolving SSTs enhance SSR variability, blue areas indicate a reduction in SSR variability. Given are multi-model median plots. Hatches indicate areas where the Mann-Whitney U test performed on the distributions of σ_{SSR} among all models is passed at a 5% significance level, i.e. the two samples come from the same distribution.

et al. (2013); P. X. Wang et al. (2017)). In mid-latitude parts of Eurasian and North American land, weather systems and year-to-year differences in the seasonal cycle may play a role. A σ_{SSR} of 4Wm^{-2}, as it is typical for wide parts of the globe under all-sky conditions, translates to an unforced trend of 2Wm^{-2}decade^{-1} sustained for 20 years (with a 10% probability chance of occurrence, 90$^{\text{th}}$ percentile of all possible trends (Folini et al., 2017; Chtirkova et al., 2022)).

As can be seen from the relative change $\sigma_{SSR,rel}$ (Figure 3 b, d), the impact of time-evolving SSTs on SSR variability is non-uniform. Over oceans, changes in SSR variability are generally more pronounced, with largest impacts of time-evolving SSTs arising in the Tropical Pacific. This finding suggests that feedback loops may exist between SSTs and SSRs, in line with literature. In fact, cloud feedbacks are of key relevance for ENSO (see e.g. Bayr and Latif (2022) and references therein) and its modeling. Middlemas et al. (2019) show, for example, that negative cloud feedbacks even control the frequency of ENSO with active feedbacks resulting in a smaller but more frequent ENSO. Over land, the increase in all-sky σ_{SSR} is on average 0.47 Wm^{-2} (11%). The change in σ_{SSR} is not statistically significant for many land areas, but is significant for a large part of the U.S., South America, West Central Africa and Australia for both all-sky and clear-sky SSR.

Looking into inter-model differences (per model plots are shown on Figure A1 for all-sky and Figure A2 for clear-sky SSR), we see that few models even show a slight but overall decrease of SSR variability above continents when using time-evolving SSTs; this indicates that within these models the atmospheric year-to-year variability over continents is suppressed by the ocean. The most pronounced decreases in inter-annual SSR variability are above Sahara and India (both all-sky and clear-sky SSR), while MPI-ESM-1-2-HAM and EC-Earth3 (r2) show a general decrease in clear-sky SSR variability above all Northern Hemispheric continents. Despite them, the majority of models show an increase of SSR variability with time-evolving SSTs above ocean and most land areas. The insufficient length of the piClim-control simulation (30 years) might be responsible for the fine-structure noise in the model-specific plots. Differences in the representation of ENSO and other modes of variability within models would contribute to the inter-model spread that is observed. The NorESM2 and GISS models which have a strong ENSO (high standard deviation of the nino3.4) also show a higher increase in $\bar{\sigma}_{SSR}$. Models with a weaker ENSO (lower standard deviation of the nino3.4 index) like BCC-ESM1, CNRM-CM6.1 and GFDL-CM4 show a smaller increase in $\bar{\sigma}_{SSR}$ for all-sky and clear-sky. On the other hand, the EC-Earth and ACCESS model families that have a weaker ENSO (lower standard deviation of the nino3.4 index), show a large increase in $\bar{\sigma}_{SSR}$ both for all-sky and clear-sky.

In summary, the above findings demonstrate a clear impact of time-evolving SSTs on SSR variability from global to regional scale. The results imply a clear increase of SSR variability due to time-variable SSTs, but they also show that SSR variability is substantial even in the absence of time-variable SSTs. Potential causes that come to mind include atmospheric variability, albedo effects via snow cover in high latitudes (through multiple scattering between the atmosphere and land surface), or also time varying aerosols. We briefly examine this last possibility in Section 3.2, but refer to the literature for dedicated studies on aerosols and their representation in models (e.g. Fanourgakis et al. (2019); Zhao et al. (2022)). A detailed analysis of these competing factors is, however, beyond the scope of this paper.

3.2 The role of aerosol concentration for SSR variability

The data presented in the previous section not only demonstrates a clear impact of time variable SSTs on SSR variability, but also raises the question about further causes, as SSR variability is high also for climatological SSTs (panels a and b in Figure 3). In this section, we examine how the mean state and the variability of SSR is affected by aerosols, notably natural aerosols: desert dust, sea salt, dimethyl sulfate (DMS) and aerosols emitted from natural fires. As detailed in Section 2.3, this analysis is constrained by the available CMIP6 data: atmosphere-only pre-industrial control experiments with doubled emissions, piClim-2x. We examine changes in mean SSR upon doubling of emissions to estimate the potential region of influence of (short lived) natural aerosols on SSR and we check whether unforced SSR variability would be greater in an atmosphere with a higher mean aerosol concentration. In addition, we investigate a few cases with anthropogenic aerosols (sulfur dioxide (SO_2), organic carbon (OC), black carbon (BC)) to inspect their relevance as compared to the natural aerosols – the perturbations involve switching to the 2014 aerosol emissions for certain constituents in an otherwise pre-industrial climate. A summary of the experiments is provided in Table 1.

We first check for any general reduction of SSR due to increased aerosol emissions. Thereby, for each experiment, we subtract the multi-model median of the sensitivity experiment (piClim-*) from the multi-model median of the control run (piClim-control). Results for mean all-sky and clear-sky SSR are shown on Figure 4, first and third column, respectively. As a different number of models participates in each experiment, we compute the control-run median based on that subset of models. The reader is advised that the data provided by modelling centres for these experiments is limited and the multi-model statistics are based on experiments involving 5 to 10 models, therefore, the results should be subject to a qualitative, rather than a quantitative analysis.

Figure 4. Differences between the piClim simulations (indicated with vertical text on the left) and the control experiment (piClim-control). First and third column show the absolute difference in the mean values per grid box in Wm^{-2} for all-sky and clear-sky SSR respectively. Second and fourth columns show the corresponding relative change in α_{SSR} (the absolute difference, divided by α_{SSR} (piClim-control) per grid box). Shown are CMIP6 multi-model medians, a different number of models is behind each subplot. Numbers in the bottom right of each subplot indicate area weighted global means in the respective dimensions.

As is to be expected, higher natural aerosol loads result in an overall reduction of SSR. Taking again the median across all models, a doubling of natural aerosol emissions reduces the long-term global mean all-sky SSR by between 3.19 Wm^{-2} in the case of sea salt and 0.60 Wm^{-2} for natural fires. Reductions for DMS and dust are 1.42 and 0.87 Wm^{-2}

around the year 2000 is probably related to the short rise in both PDO and ENSO from 1999 until 2004, which would induce brightening.

Using proxies from sunshine duration and diurnal temperature range in Iran, Rahimzadeh et al. (2014) identify dimming from early 1960s to late 1970s; brightening from early 1980s until 2000 and dimming during the 2000s until 2009. The region is influenced by the Pacific and Indian ocean modes. The strong rise in IOD$\uparrow^{1955-1965}$, PDO$\uparrow^{1950-1960}$ may have influenced the dimming; the following IOD$\downarrow^{1970-1990}$ and PDO$\downarrow^{1990-2010}$ would contribute to brightening. The observed dimming during the 2000s (not found to be statistically significant in Rahimzadeh et al. (2014)) might bear again an imprint of the strong short-term rise in PDO or ENSO 1999 until 2004, which would induce brightening in China, but dimming in Iran.

Global irradiance measurements in Israel from Stanhill and Ianetz (1997) are also found to show an overall dimming between 1955 and 1995. The filtered data time series on Fig. 1 (A) in Stanhill and Ianetz (1997) mirror the long-term fluctuations in the PDO, a rise in PDO would cause dimming in the region, and are in line with our findings that this region is influenced more strongly from the Pacific modes as compared to the Atlantic ones.

According to Figure 7, Europe is shown to have an imprint of both Atlantic modes (more in the Southwest part and in the Eastern part) and Pacific modes (more in the Central and Southern part) with the relative imprint of the Pacific modes being stronger in the Southern part. According to our results the PDO$\uparrow$ and AMO$\downarrow$ would contribute to dimming and PDO$\downarrow$ and AMO$\uparrow$ to brightening in Central, Southern and Western Europe. Dimming and brightening across Europe are documented in Sanchez-Lorenzo et al. (2015), where Figure 3 resembles the PDO phases. Namely PDO$\downarrow^{1935-1950}$ could have enhanced the early brightening between 1939-1949; PDO$\uparrow^{1950-1960}$, PDO$\uparrow^{1970-1985}$ and AMO$\downarrow^{1950-1975}$ would have contributed to the dimming between 1950-1985 with the period of weaker dimming during PDO$^{1960-1970}$; and PDO$\downarrow^{1990-2010}$ and AMO$\uparrow^{1985-2010}$ would enhance the brightening observed from 1986-2012 (see Table 3 in Sanchez-Lorenzo et al. (2015) for references). We note, however, that non-SST related internal variability is also present on the continent (see Figure 3), and the mechanisms through which Pacific SSTs affect Europe are complex (e.g. Domeisen et al. (2014); Jiménez-Esteve and Domeisen (2018)). Thus, even though our results suggest that dimming and brightening in Europe have likely been enhanced by SST-related variability, other processes might be enhancing or suppressing the effect of anthropogenic aerosols at the regional level.

5 Conclusion

Internal variability needs to be be taken into account when interpreting model simulations and real-world phenomena ranging from daily (e.g. Zeman and Schär (2022)), to decadal (e.g. Deser, Phillips, et al. (2010)) and centennial time scales (e.g. Latif et al. (2013)). This paper seeks a relationship between long-term, decadal scale, variations in SSR and long-term variations in SST for a climate without any external forcing factors where the processes occur solely due to internal variability of the climate system. We examine, on the one hand, σ_{SSR} and recall that a larger σ_{SSR} implies stronger unforced SSR trends of any length (Folini et al., 2017; Chtirkova et al., 2022). On the other hand, we examine SSR trends in periods when major climate indices undergo strong changes. The findings of the study should be taken into account when interpreting both model and observational data sets of SSR, in which the SST-related variability competes with the anthropogenic signal.

We compare year-to-year SSR variability caused by time-evolving SSTs to SSR variability only induced by the atmosphere with increased aerosol concentrations. The relative increase in variability when moving from constant climatological to time-evolving

SSTs (coupled simulations) is 30% for all-sky SSR and 25% for clear-sky SSR. Increasing the aerosol emissions (both natural and anthropogenic) results in a decline in the mean SSR but yields no significant changes in variability for all-sky SSR, thus we conclude that all-sky variability is dominated by cloud variability. For clear-sky SSR, we find changes in variability for doubling the amount of sea salt (19%), dust (9%), and natural fires (7%), as well as a considerably smaller change for DMS (1%). We also observe increases in clear-sky SSR variability for setting antropogenic aerosol emissions to present-day values as compared to pre-industrial levels: all anthropogenic aerosols (9%), SO_2 (4%), OC (2%), BC (2%). We conclude that aerosol concentrations act on all-sky SSR only through changes in the mean, but not in $_{\text{all-sky SSR}}$, while their effect on clear-sky SSR is evident in both the mean and $_{\text{clear-sky SSR}}$, i.e. unforced clear-sky SSR trends depend on the absolute amounts of aerosols in the atmosphere and are different in present-day as compared to pre-industrial climate. To describe the effect of unforced changes in SST on SSR, we use well-known climate indices because they are easily available and understandable. The compound results of the pre-industrial control runs from 69 CMIP6 simulations give insights on the direction of influence of different climate modes on all-sky and clear-sky SSR trends. We hypothesise that the largest SSR trends occur during periods of drastic changes in the climate index (when the mode switches phase). For better statistics, and to partially separate the individual effects of the separate climate modes, we average SSR trends for periods with the most drastic changes in the index. Thus, we identify patterns of decadal SSR trends associated with different climate modes which are based on SSTs. Comparing all-sky and clear-sky SSR trend patterns, we find that they are not identical: clear-sky trend patterns usually cover wider areas, are related to water vapour and have smaller magnitudes, while patterns in all-sky trends have a more complex structure often being of opposite sign to the clear-sky trend. The all-sky and clear-sky patterns that we identify suggest that the influence of SSTs on SSR involves both changes in cloudiness and in water vapour. The results concerning clear-sky variability should complement emerging efforts to derive clear-sky SSR time series from observations (Correa et al., 2022). Even though models generally under-represent internal variability, our results may be used to give a qualitative estimate whether a certain change in a climate mode has an enhancing or suppressing effect on regional dimming and brightening. The directions of influence of climate modes in different regions are summarized on Figures 7 - 8. Regions influenced by several modes also tend to show higher SSR trends.

Overall, the results presented in this paper suggest that the effect of climate modes on SSR is not random and can be inferred from the time-dependent SST field. The magnitudes of the influence are not well constrained due to model flaws but still the models seem adequate enough to deduce at least qualitatively a relation between SSR and SST changes. Comparing observed dimming and brightening around the world to the historical time series of the climate modes from 1920 until 2015, we speculate that SST-related internal variability in SSR has enhanced rather than suppressed the observed SSR trends in most regions of the world, where long term observations exist. Exceptions are India and China, where the PDO signal possibly acts in the opposite direction to the aerosol signal and might offer an explanation for the weaker brightening in all-sky as compared to clear-sky in China. Even though European dimming and brightening appears to be enhanced by SST-related internal variability on the continental scale, we do not exclude non-SST related variability playing a role and counteracting the aerosol signal at regional scales. Further quantification of the SSR trend magnitudes related to internal variability and superposition of modes can only be done using numerical simulations.

A possible domain of application of our study beyond the interpretation of observed SSR trends would be the potential role of SST modes for long-term planning of photovoltaic energy production. The links between climate modes and SSR trends, identified in this paper, can be further used to estimate long-term variability in photovoltaic energy production (e.g. Davy and Troccoli (2012); Gonzalez-Salazar and Poganietz (2021)) for different regions. For the power grid balancing, locations influenced by modes acting in opposing directions can be considered, as well as locations where internal variability is generally less.

Appendix A

Group on Coupled Modelling, coordinated and promoted CMIP6. We thank the climate modeling groups for producing and making available their model output, the Earth System Grid Federation (ESGF) for archiving the data and providing access, and the multiple funding agencies who support CMIP6 and ESGF. Many of the observational dimming/brightening studies referred to in this study profited from the Global Energy Balance Archive (GEBA) co-funded by the Federal Office of Meteorology and Climatology Meteoswiss in the context of GCOS Switzerland. The data analysis and visualization have been performed using exclusively free and open source software (including Linux, Python and CDO): we would like to thank the community for building powerful tools from which everyone can benefit. We also thank the three anonymous reviewers for their constructive comments which helped improving the manuscript.

Open Research

The CMIP6 data may be accessed at `https://esgf-node.llnl.gov/projects/cmip6/` (Eyring et al., 2016). The CVDP package and associated data are available at `https://www.cesm.ucar.edu/projects/cvdp` (Phillips et al., 2014). NOAA Extended Reconstructed SST V5 (ERSST) data is avaibalbe from `https://psl.noaa.gov/data/gridded/data.noaa.ersst.v5.html` (Huang et al., 2017).

References

Antuña, J. C., Fonte, A., Rodríguez, A., & Wild, M. (2011). Observed solar dimming in the wider caribbean. *Atmósfera*, *24*(2). Retrieved from `https://www.revistascca.unam.mx/atm/index.php/atm/article/view/24827`

Augustine, J. A., & Capotondi, A. (2022). Forcing for multidecadal surface solar radiation trends over northern hemisphere continents. *Journal of Geophysical Research: Atmospheres*, *127*(16), e2021JD036342. Retrieved from `https://agupubs.onlinelibrary.wiley.com/doi/abs/10.1029/2021JD036342` (e2021JD036342 2021JD036342) doi: https://doi.org/10.1029/2021JD036342

Augustine, J. A., & Hodges, G. B. (2021, April). Variability of surface radiation budget components over the u.s. from 1996 to 2019—has brightening ceased? *Journal of Geophysical Research: Atmospheres*, *126*(7). Retrieved from `https://doi.org/10.1029/2020jd033590` doi: 10.1029/2020jd033590

Bayr, T., & Latif, M. (2022, August). ENSO atmospheric feedbacks under global warming and their relation to mean-state changes. *Climate Dynamics*, *60*(9-10), 2613–2631. Retrieved from `https://doi.org/10.1007/s00382-022-06454-3` doi: 10.1007/s00382-022-06454-3

Chiacchio, M., & Wild, M. (2010). Influence of nao and clouds on long-term seasonal variations of surface solar radiation in europe. *Journal of Geophysical Research: Atmospheres*, *115*(D10). Retrieved from `https://agupubs.onlinelibrary.wiley.com/doi/abs/10.1029/2009JD012182` doi: https://doi.org/10.1029/2009JD012182

Chtirkova, B., Folini, D., Correa, L. F., & Wild, M. (2022, 6). Internal variability of all-sky and clear-sky surface solar radiation on decadal timescales. *Journal of Geophysical Research: Atmospheres*, *127*, e2021JD036332. Retrieved from `https://onlinelibrary.wiley.com/doi/abs/10.1029/2021JD036332` doi: 10.1029/2021JD036332

Coburn, J., & Pryor, S. C. (2021, 10). Differential credibility of climate modes in cmip6. *Journal of Climate*, *34*, 8145-8164. Retrieved from `https://journals.ametsoc.org/view/journals/clim/34/20/JCLI-D-21-0359.1.xml` doi: 10.1175/JCLI-D-21-0359.1

Correa, L. F., Folini, D., Chtirkova, B., & Wild, M. (2022, August). A method for clear-sky identification and long-term trends assessment using daily surface solar radiation records. *Earth and Space Science*, *9*(8). Retrieved from https://doi.org/10.1029/2021ea002197 doi: 10.1029/2021ea002197

Davy, R. J., & Troccoli, A. (2012, December). Interannual variability of solar energy generation in australia. *Solar Energy*, *86*(12), 3554–3560. Retrieved from https://doi.org/10.1016/j.solener.2011.12.004 doi: 10.1016/j.solener.2011.12.004

Deser, C., Alexander, M. A., Xie, S.-P., & Phillips, A. S. (2010). Sea surface temperature variability: Patterns and mechanisms. *Annual Review of Marine Science*, *2*(1), 115-143. Retrieved from https://doi.org/10.1146/annurev-marine-120408-151453 (PMID: 21141660) doi: 10.1146/annurev-marine-120408-151453

Deser, C., Phillips, A., Bourdette, V., & Teng, H. (2010, dec). Uncertainty in climate change projections: the role of internal variability. *Clim Dyn*, *38*(3-4), 527–546. Retrieved from https://doi.org/10.1007%2Fs00382-010-0977-x doi: 10.1007/s00382-010-0977-x

Deser, C., Phillips, A. S., & Hurrell, J. W. (2004). Pacific interdecadal climate variability: Linkages between the tropics and the north pacific during boreal winter since 1900. *Journal of Climate*, *17*(16), 3109 - 3124. Retrieved from https://journals.ametsoc.org/view/journals/clim/17/16/1520-0442_2004_017_3109_picvlb_2.0.co_2.xml doi: 10.1175/1520-0442(2004)017⟨3109:PICVLB⟩2.0.CO;2

Domeisen, D. I. V., Butler, A. H., Fröhlich, K., Bittner, M., Müller, W. A., & Baehr, J. (2014, December). Seasonal predictability over europe arising from el niño and stratospheric variability in the MPI-ESM seasonal prediction system. *Journal of Climate*, *28*(1), 256–271. Retrieved from https://doi.org/10.1175/jcli-d-14-00207.1 doi: 10.1175/jcli-d-14-00207.1

Eyring, V., Bony, S., Meehl, G. A., Senior, C. A., Stevens, B., Stouffer, R. J., & Taylor, K. E. (2016, may). Overview of the coupled model intercomparison project phase 6 (CMIP6) experimental design and organization. *Geosci. Model Dev.*, *9*(5), 1937–1958. Retrieved from https://doi.org/10.5194%2Fgmd-9-1937-2016 doi: 10.5194/gmd-9-1937-2016

Fanourgakis, G. S., Kanakidou, M., Nenes, A., Bauer, S. E., Bergman, T., Carslaw, K. S., ... Yu, F. (2019, July). Evaluation of global simulations of aerosol particle and cloud condensation nuclei number, with implications for cloud droplet formation. *Atmospheric Chemistry and Physics*, *19*(13), 8591–8617. Retrieved from https://doi.org/10.5194/acp-19-8591-2019 doi: 10.5194/acp-19-8591-2019

Fasullo, J. T., Phillips, A. S., & Deser, C. (2020, 7). Evaluation of leading modes of climate variability in the cmip archives. *Journal of Climate*, *33*, 5527-5545. Retrieved from https://journals.ametsoc.org/view/journals/clim/33/13/jcli-d-19-1024.1.xml doi: 10.1175/JCLI-D-19-1024.1

Folini, D., Dallafior, T. N., Hakuba, M. Z., & Wild, M. (2017, jan). Trends of surface solar radiation in unforced CMIP5 simulations. *J. Geophys. Res. Atmos.*, *122*(1), 469–484. Retrieved from https://doi.org/10.1002%2F2016jd025869 doi: 10.1002/2016jd025869

Folini, D., & Wild, M. (2011, November). Aerosol emissions and dimming/brightening in europe: Sensitivity studies with ECHAM5-HAM. *Journal of Geophysical Research: Atmospheres*, *116*(D21). Retrieved from https://doi.org/10.1029/2011jd016227 doi: 10.1029/2011jd016227

Folini, D., & Wild, M. (2015). The effect of aerosols and sea surface temperature on china's climate in the late twentieth century from ensembles of global climate simulations. *Journal of Geophysical Research*, *120*, 2261-2279. doi: 10.1002/2014JD022851

Gonzalez-Salazar, M., & Poganietz, W. R. (2021, August). Evaluating the complementarity of solar, wind and hydropower to mitigate the impact of el niño southern oscillation in latin america. *Renewable Energy*, *174*, 453–467.

Retrieved from https://doi.org/10.1016/j.renene.2021.04.048 doi: 10.1016/j.renene.2021.04.048

Hourdin, F., Mauritsen, T., Gettelman, A., Golaz, J.-C., Balaji, V., Duan, Q., ... Williamson, D. (2017). The art and science of climate model tuning. *Bulletin of the American Meteorological Society*, *98*(3), 589 - 602. Retrieved from https://journals.ametsoc.org/view/journals/bams/98/3/bams-d-15-00135.1.xml doi: 10.1175/BAMS-D-15-00135.1

Huang, B., Thorne, P. W., Banzon, V. F., Boyer, T., Chepurin, G., Lawrimore, J. H., ... Zhang, H.-M. (2017). *Noaa extended reconstructed sea surface temperature (ersst), version 5.* NOAA National Centers for Environmental Information. Retrieved from https://data.nodc.noaa.gov/cgi-bin/iso?id=gov.noaa.ncdc:C00927 doi: 10.7289/V5T72FNM

IPCC. (2021). *Climate change 2021: The physical science basis. contribution of working group i to the sixth assessment report of the intergovernmental panel on climate change* [Book]. Cambridge, United Kingdom and New York, NY, USA: Cambridge University Press. Retrieved from https://www.ipcc.ch/report/ar6/wg1/

Jiménez-Esteve, B., & Domeisen, D. I. V. (2018). The tropospheric pathway of the enso–north atlantic teleconnection. *Journal of Climate*, *31*(11), 4563 - 4584. Retrieved from https://journals.ametsoc.org/view/journals/clim/31/11/jcli-d-17-0716.1.xml doi: 10.1175/JCLI-D-17-0716.1

Laepple, T., & Huybers, P. (2014a, April). Global and regional variability in marine surface temperatures. *Geophysical Research Letters*, *41*(7), 2528–2534. Retrieved from https://doi.org/10.1002/2014gl059345 doi: 10.1002/2014gl059345

Laepple, T., & Huybers, P. (2014b, November). Ocean surface temperature variability: Large model–data differences at decadal and longer periods. *Proceedings of the National Academy of Sciences*, *111*(47), 16682–16687. Retrieved from https://doi.org/10.1073/pnas.1412077111 doi: 10.1073/pnas.1412077111

Lapointe, F., Bradley, R. S., Francus, P., Balascio, N. L., Abbott, M. B., Stoner, J. S., ... Labarre, T. (2020, October). Annually resolved atlantic sea surface temperature variability over the past 2, 900 y. *Proceedings of the National Academy of Sciences*, *117*(44), 27171–27178. Retrieved from https://doi.org/10.1073/pnas.2014166117 doi: 10.1073/pnas.2014166117

Latif, M., Martin, T., & Park, W. (2013, September). Southern ocean sector centennial climate variability and recent decadal trends. *Journal of Climate*, *26*(19), 7767–7782. Retrieved from https://doi.org/10.1175/jcli-d-12-00281.1 doi: 10.1175/jcli-d-12-00281.1

Lee, J., Sperber, K. R., Gleckler, P. J., Taylor, K. E., & Bonfils, C. J. W. (2021, May). Benchmarking performance changes in the simulation of extratropical modes of variability across CMIP generations. *Journal of Climate*, 1–70. Retrieved from https://doi.org/10.1175/jcli-d-20-0832.1 doi: 10.1175/jcli-d-20-0832.1

Liley, J. B. (2009, April). New zealand dimming and brightening. *Journal of Geophysical Research*, *114*. Retrieved from https://doi.org/10.1029/2008jd011401 doi: 10.1029/2008jd011401

Lindzen, R. S., & Nigam, S. (1987, September). On the role of sea surface temperature gradients in forcing low-level winds and convergence in the tropics. *Journal of the Atmospheric Sciences*, *44*(17), 2418–2436. Retrieved from https://doi.org/10.1175/1520-0469(1987)044<2418:otross>2.0.co;2 doi: 10.1175/1520-0469(1987)044⟨2418:otross⟩2.0.co;2

Liu, S., Zeman, C., Sørland, S. L., & Schär, C. (2022, November). Systematic calibration of a convection-resolving model: Application over tropical atlantic. *Journal of Geophysical Research: Atmospheres*. Retrieved from https://doi.org/10.1029/2022jd037303 doi: 10.1029/2022jd037303

Loeb, N. G., Kato, S., Su, W., Wong, T., Rose, F. G., Doelling, D. R., ... Huang, X. (2012, January). Advances in understanding top-of-atmosphere radiation variability from satellite observations. *Surveys in Geophysics*, *33*(3-4), 359–385. Retrieved from https://doi.org/10.1007/s10712-012-9175-1 doi: 10.1007/s10712-012-9175-1

Loeb, N. G., Thorsen, T., Norris, J., Wang, H., & Su, W. (2018, July). Changes in earth's energy budget during and after the "pause" in global warming: An observational perspective. *Climate*, *6*(3), 62. Retrieved from https://doi.org/10.3390/cli6030062 doi: 10.3390/cli6030062

Loeb, N. G., Wang, H., Allan, R. P., Andrews, T., Armour, K., Cole, J. N. S., ... Wyser, K. (2020, March). New generation of climate models track recent unprecedented changes in earth's radiation budget observed by CERES. *Geophysical Research Letters*, *47*(5). Retrieved from https://doi.org/10.1029/2019gl086705 doi: 10.1029/2019gl086705

Mann, H. B., & Whitney, D. R. (1947, March). On a test of whether one of two random variables is stochastically larger than the other. *The Annals of Mathematical Statistics*, *18*(1), 50–60. Retrieved from https://doi.org/10.1214/aoms/1177730491 doi: 10.1214/aoms/1177730491

Middlemas, E. A., Clement, A. C., Medeiros, B., & Kirtman, B. (2019, July). Cloud radiative feedbacks and el niño–southern oscillation. *Journal of Climate*, *32*(15), 4661–4680. Retrieved from https://doi.org/10.1175/jcli-d-18-0842.1 doi: 10.1175/jcli-d-18-0842.1

Phillips, A. S., Deser, C., & Fasullo, J. (2014). A new tool for evaluating modes of variability in climate models. *EOS*, *95*, 453–455. Retrieved from https://www.cesm.ucar.edu/working_groups/CVC/cvdp/ doi: 10.1002/2014EO490002

Pinker, R. T., Grodsky, S. A., Zhang, B., Busalacchi, A., & Chen, W. (2017). Enso impact on surface radiative fluxes as observed from space. *Journal of Geophysical Research: Oceans*, *122*(10), 7880-7896. Retrieved from https://agupubs.onlinelibrary.wiley.com/doi/abs/10.1002/2017JC012900 doi: https://doi.org/10.1002/2017JC012900

Power, H. C., & Mills, D. M. (2005). Solar radiation climate change over southern africa and an assessment of the radiative impact of volcanic eruptions. *International Journal of Climatology*, *25*(3), 295–318. Retrieved from https://doi.org/10.1002/joc.1134 doi: 10.1002/joc.1134

Rahimzadeh, F., Sanchez-Lorenzo, A., Hamedi, M., Kruk, M. C., & Wild, M. (2014, July). New evidence on the dimming/brightening phenomenon and decreasing diurnal temperature range in iran (1961-2009). *International Journal of Climatology*, *35*(8), 2065–2079. Retrieved from https://doi.org/10.1002/joc.4107 doi: 10.1002/joc.4107

Raichijk, C. (2011, January). Observed trends in sunshine duration over south america. *International Journal of Climatology*, *32*(5), 669–680. Retrieved from https://doi.org/10.1002/joc.2296 doi: 10.1002/joc.2296

Sanchez-Lorenzo, A., Wild, M., Brunetti, M., Guijarro, J. A., Hakuba, M. Z., Calbó, J., ... Bartok, B. (2015). Reassessment and update of long-term trends in downward surface shortwave radiation over europe (1939–2012). *Journal of Geophysical Research: Atmospheres*, *120*(18), 9555-9569. Retrieved from https://agupubs.onlinelibrary.wiley.com/doi/abs/10.1002/2015JD023321 doi: https://doi.org/10.1002/2015JD023321

Schwarz, M., Folini, D., Hakuba, M. Z., & Wild, M. (2018, December). From point to area: Worldwide assessment of the representativeness of monthly surface solar radiation records. *Journal of Geophysical Research: Atmospheres*, *123*(24). Retrieved from https://doi.org/10.1029/2018jd029169 doi: 10.1029/2018jd029169

Smith, C. J., Kramer, R. J., Myhre, G., Alterskjær, K., Collins, W., Sima, A., ...

Forster, P. M. (2020, January). Effective radiative forcing and adjustments in CMIP6 models. Retrieved from https://doi.org/10.5194/acp-2019-1212 doi: 10.5194/acp-2019-1212

Soni, V. K., Pandithurai, G., & Pai, D. S. (2011, January). Evaluation of long-term changes of solar radiation in india. *International Journal of Climatology*, *32*(4), 540–551. Retrieved from https://doi.org/10.1002/joc.2294 doi: 10.1002/joc.2294

Stanhill, G., & Ianetz, A. (1997, January). Long-term trends in, and the spatial variation of, global irradiance in israel. *Tellus B: Chemical and Physical Meteorology*, *49*(1), 112. Retrieved from https://doi.org/10.3402/tellusb.v49i1.15954 doi: 10.3402/tellusb.v49i1.15954

Stephens, G. L., Hakuba, M. Z., Webb, M. J., Lebsock, M., Yue, Q., Kahn, B. H., ... Slingo, J. (2018, May). Regional intensification of the tropical hydrological cycle during ENSO. *Geophysical Research Letters*, *45*(9), 4361–4370. Retrieved from https://doi.org/10.1029/2018gl077598 doi: 10.1029/2018gl077598

Streets, D. G., Wu, Y., & Chin, M. (2006). Two-decadal aerosol trends as a likely explanation of the global dimming/brightening transition. *Geophys. Res. Lett.*, *33*(15). Retrieved from https://doi.org/10.1029%2F2006gl026471 doi: 10.1029/2006gl026471

Thornhill, G., Collins, W., Olivié, D., Skeie, R. B., Archibald, A., Bauer, S., ... Weber, J. (2021, January). Climate-driven chemistry and aerosol feedbacks in CMIP6 earth system models. *Atmospheric Chemistry and Physics*, *21*(2), 1105–1126. Retrieved from https://doi.org/10.5194/acp-21-1105-2021 doi: 10.5194/acp-21-1105-2021

Vimont, D. J. (2005). The contribution of the interannual enso cycle to the spatial pattern of decadal enso-like variability. *Journal of Climate*, *18*(12), 2080 - 2092. Retrieved from https://journals.ametsoc.org/view/journals/clim/18/12/jcli3365.1.xml doi: 10.1175/JCLI3365.1

Wang, P. X., Wang, B., Cheng, H., Fasullo, J., Guo, Z., Kiefer, T., & Liu, Z. (2017, November). The global monsoon across time scales: Mechanisms and outstanding issues. *Earth-Science Reviews*, *174*, 84–121. Retrieved from https://doi.org/10.1016/j.earscirev.2017.07.006 doi: 10.1016/j.earscirev.2017.07.006

Wang, Y., & Wild, M. (2016, November). A new look at solar dimming and brightening in china. *Geophysical Research Letters*, *43*(22). Retrieved from https://doi.org/10.1002/2016gl071009 doi: 10.1002/2016gl071009

Wild, M. (2009, June). Global dimming and brightening: A review. *Journal of Geophysical Research*, *114*. Retrieved from https://doi.org/10.1029/2008jd011470 doi: 10.1029/2008jd011470

Wild, M. (2012, January). Enlightening global dimming and brightening. *Bulletin of the American Meteorological Society*, *93*(1), 27–37. Retrieved from https://doi.org/10.1175/bams-d-11-00074.1 doi: 10.1175/bams-d-11-00074.1

Wild, M., Gilgen, H., Roesch, A., Ohmura, A., Long, C. N., Dutton, E. G., ... Tsvetkov, A. (2005, May). From dimming to brightening: Decadal changes in solar radiation at earth's surface. *Science*, *308*(5723), 847–850. Retrieved from https://doi.org/10.1126/science.1103215 doi: 10.1126/science.1103215

Wild, M., Wacker, S., Yang, S., & Sanchez-Lorenzo, A. (2021, March). Evidence for clear-sky dimming and brightening in central europe. *Geophysical Research Letters*, *48*(6). Retrieved from https://doi.org/10.1029/2020gl092216 doi: 10.1029/2020gl092216

Wills, R. C. J., Armour, K. C., Battisti, D. S., Proistosescu, C., & Parsons, L. A. (2021, November). Slow modes of global temperature variability and their impact on climate sensitivity estimates. *Journal of Climate*, *34*(21), 8717–8738. Retrieved from https://doi.org/10.1175/jcli-d-20-1013.1 doi: 10.1175/jcli-d-20-1013.1

Yang, S., Wang, X. L., & Wild, M. (2018, May). Homogenization and trend analysis of the 1958–2016 in situ surface solar radiation records in china. *Journal of Climate*, *31*(11), 4529–4541. Retrieved from `https://doi.org/10.1175/jcli-d-17-0891.1` doi: 10.1175/jcli-d-17-0891.1

Yang, S., Wang, X. L., & Wild, M. (2019, August). Causes of dimming and brightening in china inferred from homogenized daily clear-sky and all-sky in situ surface solar radiation records (1958–2016). *Journal of Climate*, *32*(18), 5901–5913. Retrieved from `https://doi.org/10.1175/jcli-d-18-0666.1` doi: 10.1175/jcli-d-18-0666.1

Yim, S.-Y., Wang, B., Liu, J., & Wu, Z. (2013, October). A comparison of regional monsoon variability using monsoon indices. *Climate Dynamics*, *43*(5-6), 1423–1437. Retrieved from `https://doi.org/10.1007/s00382-013-1956-9` doi: 10.1007/s00382-013-1956-9

Zeman, C., & Schär, C. (2022, April). An ensemble-based statistical methodology to detect differences in weather and climate model executables. *Geoscientific Model Development*, *15*(8), 3183–3203. Retrieved from `https://doi.org/10.5194/gmd-15-3183-2022` doi: 10.5194/gmd-15-3183-2022

Zhao, A., Ryder, C. L., & Wilcox, L. J. (2022, February). How well do the CMIP6 models simulate dust aerosols? *Atmospheric Chemistry and Physics*, *22*(3), 2095–2119. Retrieved from `https://doi.org/10.5194/acp-22-2095-2022` doi: 10.5194/acp-22-2095-2022